J. Plasma Phys. (2019), *vol.* 85, 905850102
doi:10.1017/S0022377818001356

Longitudinal characterization of the wake and electron bunch in a laser wakefield accelerator

Zhijun Zhang[1], Wentao Wang[1], Jiansheng Liu[1,2,3,4,†], Ming Fang[1], Wentao Li[1], Ye Tian[1], Rong Qi[1], Cheng Wang[1], Changhai Yu[1], Zhiyong Qin[1], Jiaqi Liu[1], Ruxin Li[1] and Zhizhan Xu[1]

[1]State Key Laboratory of High Field Laser Physics, Shanghai Institute of Optics and Fine Mechanics, Chinese Academy of Sciences, Shanghai 201800, China

[2]Department of Physics, Shanghai Normal University, Shanghai 200234, China

[3]Institute of Modern Optics, Nankai University, Tianjing 300000, PR China

[4]Collaborative Innovation Center of IFSA (CICIFSA), Shanghai Jiao Tong University, Shanghai 200240, China

(Received 19 July 2018; revised 6 December 2018; accepted 10 December 2018)

Energy chirp compensation of the electron bunch (e-bunch) in a laser wakefield accelerator, which is caused by the phase space rotation in the gradient wakefield, has been applied in many schemes for low energy spread e-bunch generation. We report the experimental observation of energy chirp compensation of the e-bunch in a nonlinear laser wakefield accelerator with a negligible beam loading effect. By adjusting the acceleration length using a wedge-roof block, the chirp compensation of the accelerated e-bunch was observed via an electron spectrometer. Apart from this, some significant parameters for the compensation process, such as the longitudinal dispersion and wakefield slope at the bunch position, were also estimated. A detailed comparison between experiment and simulation shows good agreement of the wakefield and bunch parameters. These results give a clear demonstration of the longitudinal characteristics of the wakefield in a plasma and the bunch dynamics, which are important for better control of a compact laser wakefield accelerator.

Key words: intense particle beams, plasma applications, plasma waves

1. Introduction

Laser wakefield accelerators (LWFAs), which could sustain extreme field gradients of the order of 100 GV m^{-1}, are promising as compact sources of ultrashort e-bunches (Tajima & Dawson 1979; Lu *et al.* 2011; Liu *et al.* 2011; Kim *et al.* 2013; Wang *et al.* 2013*a*,*b*; Leemans *et al.* 2014). By applying new techniques to control the injection or the acceleration processes of a LWFA (Faure *et al.* 2006; Oz *et al.* 2007; Geddes *et al.* 2008; Rechatin *et al.* 2009*b*; Faure *et al.* 2010; Pak *et al.* 2010; Gonsalves *et al.* 2011; Bourgeois, Cowley & Hooker 2013; Xi *et al.* 2013; Buck *et al.* 2013; Litos *et al.* 2014; Zhang *et al.* 2015; Zeng *et al.* 2015; Liu *et al.* 2011;

†Email address for correspondence: michaeljs_liu@siom.ac.cn

Pollock *et al.* 2011; Steinke *et al.* 2016), remarkable progress has been made for quasi-monoenergetic and high energy (several GeV) e-bunch generation. Whereas for applications such as ultrashort x- and γ-ray sources from Compton scattering, wiggler or novel free electron laser schemes (Jaroszynski *et al.* 2006; Schwoerer *et al.* 2006; Schlenvoigt *et al.* 2007; Fuchs *et al.* 2009; Huang, Ding & Schroeder 2012; Phuoc *et al.* 2012; Chen *et al.* 2013; Powers *et al.* 2014), the e-bunch quality and stability still need to be improved.

In many previous simulation works (Tsung *et al.* 2004; Kalmykov *et al.* 2011, 2015), the phase space rotation of the e-bunch due to the gradient acceleration field in a plasma-based accelerator was used for energy spread reduction, generating e-bunches with high energy and low energy spread. In some schemes, the plasma density and the bunch phase were operated carefully to attain precise control over the phase space rotation, then a controllable energy chirp compensation or energy spread mitigation could be fulfilled at a desired energy (Brinkmann *et al.* 2017; Manahan *et al.* 2017). On the other hand, the rotation could be suppressed by flattening the wakefield with a proper tailing beam loading (Tzoufras *et al.* 2008; Litos *et al.* 2014). In our previous work (Zhang *et al.* 2016), the phase space rotation was applied to compress the longitudinal distribution of the bunch for a more efficient energy spread minimization. Since the rotation is strongly correlated with the wakefield characteristics and the bunch phase space distribution, it is meaningful to explore the rotation process both in theory and experiment.

Here in this paper, we investigate the phase space rotation of e bunches in a LWFA, which is in the nonlinear regime with a negligible beam loading effect, by altering the acceleration length (plasma length) experimentally, and present valid estimations of the wake characteristic parameters (longitudinal dispersion and slope) and the bunch length via the measured energy spectra. The resulting energy spread compensation at the beginning of acceleration was obtained. Three-dimensional (3-D) particle-in-cell (PIC) simulations show that the energy spread of an e-bunch evolves as a result of phase space rotation in the gradient wakefield, and the energy spread of an e-bunch with proper energy chirp could be compensated while being accelerated. The correlations of the bunch parameters (length, energy, energy spread) and the wake parameters are analysed in a phenomenological way, applied in our experiments for wake and bunch parameters estimation, and the results are proven to be credible. The discrepancies between the theory and experiment are also discussed.

2. Phenomenological description of the wake and e-bunch in a LWFA

Firstly, we give a phenomenological description of the phase space rotation of an e-bunch accelerated in a LWFA, and discuss the simplified correlations of the bunch parameters and the wake parameters. As shown in figure 1, the plasma wake is driven by the intense laser pulse while it enters an underdense plasma. In a nonlinear case, the acceleration field could be regarded as a linear gradient field along the propagation direction (Kostyukov, Pukhov & Kiselev 2004; Lu *et al.* 2007), and an e-bunch with longitudinal length of l_b accelerated in such a field would experience a field dispersion $\Delta E_x = E_{\text{front}} - E_{\text{back}}$, where E_{front} (E_{back}) denotes the electric field at the front (back) of the e bunch. The field dispersion could also be expressed as $\Delta E_x = E' l_b$, where E' presents the wakefield slope. The phase space of the e-bunch would rotate in such a field and its energy spectrum evolves simultaneously, as shown in figure 1(*c*). Unlike in a plasma wake driven by a charged particle beam, the relativistic e-bunch accelerated in a LWFA would undergo dephasing because

https://doi.org/10.1017/S0022377818001356 Published online by Cambridge University Press

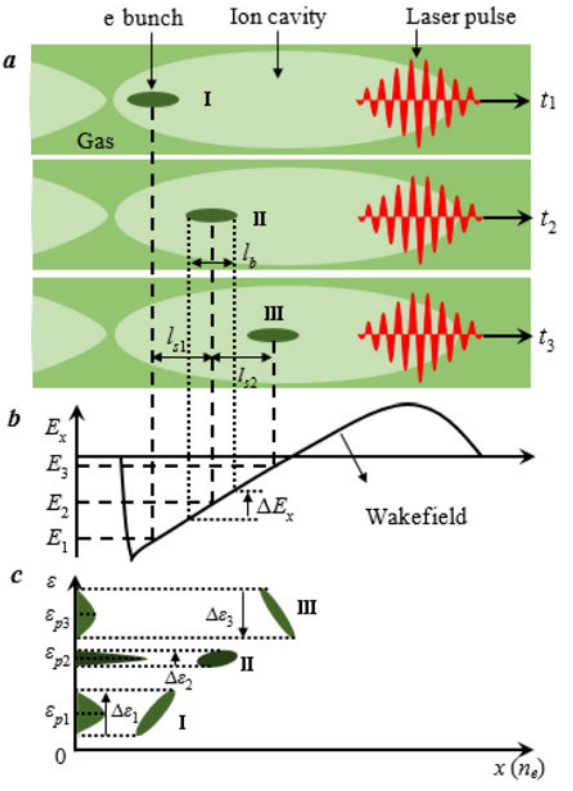

FIGURE 1. Schematic of e-bunch phase space rotation in a LWFA. (*a*) The slippages of the e-bunch with respect to the plasma wake driven by a laser pulse with different propagation times (t_1, t_2, t_3). (*b*) The wakefield on axis in the ion cavity and the wakefield dispersion ΔE_x for the e bunch. (*c*) The corresponding energy distribution and energy spectrum for the e-bunch at different times.

the group velocity of the laser pulse in the plasma is lower than the velocity of the e-bunch. Thus, the e-bunch would slip forward with respect to the wakefield, as shown in figure 1(*a*). The phase velocity of the plasma wave is $v_p \approx c[1-3\omega_p^2/(2\omega_0^2)]$ (Lu *et al.* 2007), where c is the light speed in vacuum, ω_p is the plasma frequency and ω_0 denotes the laser frequency. The slippage distance l_{s12} (t_1 to t_2), l_{s23} (t_2 to t_3) after a corresponding acceleration length of l_{a12} (t_1 to t_2), l_{a23} (t_2 to t_3) can therefore be expressed as

$$l_{s12} = l_{a12}\left(1-\frac{v_p}{c}\right) \approx \frac{3\omega_p^2}{2\omega_0^2} l_{a12}, \tag{2.1a}$$

$$l_{s23} = l_{a23}\left(1-\frac{v_p}{c}\right) \approx \frac{3\omega_p^2}{2\omega_0^2} l_{a23}. \tag{2.1b}$$

Inevitably, the bunch slippage would lead to a change of the acceleration field that the e-bunch witnesses, as shown in figure 1(*b*). For simplification, the deformation of the ion cavities during acceleration is neglected so that E' is a constant. Then, the wakefield slope E' could be deduced from the acceleration field variation together with

https://doi.org/10.1017/S0022377818001356 Published online by Cambridge University Press

the corresponding slippage distance,

$$E' \approx \frac{E_3 - E_1}{l_{s12} + l_{s23}} = 2\frac{(E_3 + E_2)/2 - (E_1 + E_2)/2}{l_{s12} + l_{s23}}, \tag{2.2}$$

where E_1, E_2 and E_3, which determine the evolution of the e-bunch's peak energy ε_p, are the acceleration fields that the density peak of the e-bunch witnesses, as shown in figure 1(*b*). The average acceleration field, which is defined as the mean value of the electric field the e-bunch witnesses during the acceleration process, could be estimated from the variation of the peak energy

$$\bar{E}_{12} = -\frac{\varepsilon_{p2} - \varepsilon_{p1}}{e l_{a12}} \approx \frac{E_1 + E_2}{2}, \tag{2.3a}$$

$$\bar{E}_{23} = -\frac{\varepsilon_{p3} - \varepsilon_{p2}}{e l_{a23}} \approx \frac{E_2 + E_3}{2}, \tag{2.3b}$$

where ε_{p1}, ε_{p2} and ε_{p3} are the corresponding peak energy of the e-bunch at t_1, t_2 and t_3, e is the elementary charge.

On the other hand, the energy spread evolution is available from the detected energy spectra, and then ΔE_x can be estimated. Since the injected e-bunch is negatively chirped (lower energy at the tail), an e-bunch in a wakefield with $\Delta E_x < 0$ will undergo energy chirp compensation at the beginning of acceleration and consequently the energy spread is compensated. After the energy chirp compensation, the energy chirp of the e-bunch would be inverted and the energy spread would be enlarged, thus a broader spectrum would be measured, as shown in figure 1(*c*). We define energy spread $\Delta\varepsilon$ as $\Delta\varepsilon = \varepsilon_{\text{front}} - \varepsilon_{\text{back}}$, then the wakefield dispersion for the e bunch could also be expressed as

$$\Delta E_x \approx \frac{\Delta\varepsilon_1 - \Delta\varepsilon_3}{e(l_{a12} + l_{a23})}, \tag{2.4}$$

where $\Delta\varepsilon_1$, $\Delta\varepsilon_2$ and $\Delta\varepsilon_3$ are the energy spread of the e-bunch at different times. By integrating the above equations together with $\Delta E_x = E' l_b$, we can estimate the e-bunch length as

$$l_b \approx \frac{3\omega_p^2}{4\omega_0^2} \frac{(\Delta\varepsilon_1 - \Delta\varepsilon_3) l_{a12} l_{a23}}{(\varepsilon_{p2} - \varepsilon_{p3}) l_{a12} - (\varepsilon_{p1} - \varepsilon_{p2}) l_{a23}}. \tag{2.5}$$

3. Experimental results

Figure 2 shows the experimental set up. Pulses from a high-repetition 200 TW Ti:sapphire (Xu *et al.* 2016) laser facility (800 nm, 33 fs, 80–90 TW on target) are focused into the gas by an $f/30$ off-axis paraboloid mirror, and the full width at half-maximum (FWHM) spot size of was measured to be $w_{\text{FWHM}} = 32$ μm in vacuum. The fractional laser energy contained within the laser spot was measured to be ∼60 % at $1/e^2$, and the normalized amplitude was estimated to be $a_0 \approx 1.2$. The target was manipulated by a pulsed gas jet with an attached plate, the diameter of the jet is 1.5 mm. A wedge-roof block with a thickness of 0.8 mm, which was connected to a motorized precision translation stage to alter the distance from the block to the plate, could split the gas to the sides so that the plasma length could be controlled. Both the plate and the block were designed with a hole of radius of 250 μm to let the laser

https://doi.org/10.1017/S0022377818001356 Published online by Cambridge University Press

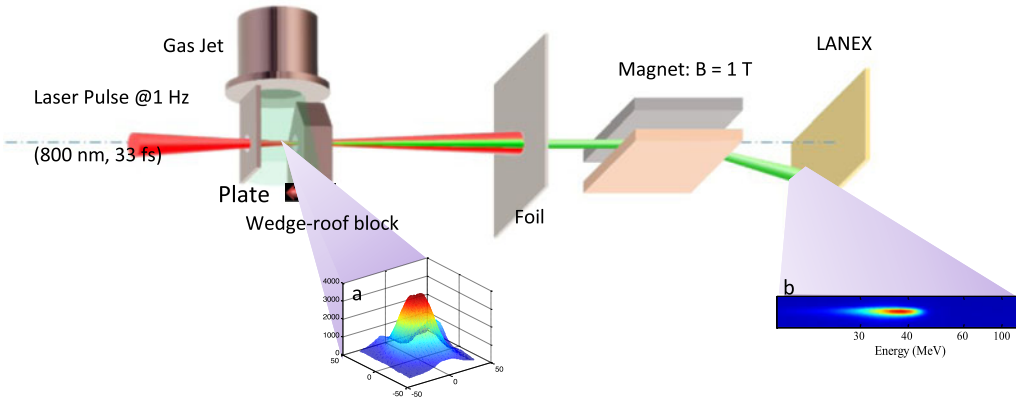

FIGURE 2. Schematic of the experimental set up. (*a*) The transverse intensity distribution of the laser pulse at the focus, the spot size is measured as 32 μm at FWHM. (*b*) A typical spectrum for e-bunch detected from the spectrometer.

pass. The plasma density profiles were measured using a probe pulse, which is split from the main pulse, directed perpendicularly through the gas jet to a Michelson-type interferometer. The gas jet was filled with pure He atoms, and the plasma density was measured to be approximately 1.0×10^{19} cm^{-3} with an accuracy of ±6 % after being totally ionized (Zhou *et al.* 2010; Wang *et al.* 2013*a*), as shown in figure 3(*a*,*b*).

The electron spectra were measured by using a 13 cm long 1 T dipole magnet which is 32 cm downstream of the gas target to bend the electron trace, and then imaged on a LANEX phosphor screen captured by an intensified charge-coupled device (ICCD). The energy resolution of the magnet spectrometer, which is determined by the transverse profile of the e-bunch, was 1.6 % at 100 MeV. The uncertainty of the measured electron energy was estimated according to a shot-to-shot e-bunch divergence of 1.0 mrad, which is derived based on the standard deviation of the positions of the straight through reference shots when the magnet was removed, leading to an error of [2.1 MeV, −1.6 MeV] at 100 MeV. The e-bunch charge was cross-calibrated by using a calibrated imaging plate (Bonnet *et al.* 2013). The uncertainty of the measured e-bunch charge was estimated to be within ±12 %. The spectra are cut off at around 20 MeV due to the imaging range limitation of the ICCD, and only the shots for which the charge deviation between the experiment and the corresponding Gaussian fitting are less than 20 % are selected.

In the experiments, we altered the distance l (from the block front edge to the attached plate) from 0.8 to 1.2 mm by adjusting the position of the wedge-roof block, l was chosen to be much less than the depletion length (approximately 2.5 mm under the experimental condition) to avoid the disruption of the e-bunch longitudinal bunch profile (Heigoldt *et al.* 2015), and the generated electron spectra are shown in figure 3(*c*–*f*). Although no special injection control techniques like ionization or density transition were applied in our experiment, the generated e-bunches were quasi-monoenergetic. This might be attributable to the first self-injection at the very front of the plasma (Corde *et al.* 2013), where the injection process was confined within a very limited time. Ten shots of e-bunch spectra for each of three runs with different l are shown in figure 3(*c*–*e*), and the statistical spectra parameters are listed in table 1, the errors are root-mean-square (r.m.s.) deviations from the average value. For the spectra in figure 3(*f*) and the data in table 1, the later injected bunches at

https://doi.org/10.1017/S0022377818001356 Published online by Cambridge University Press

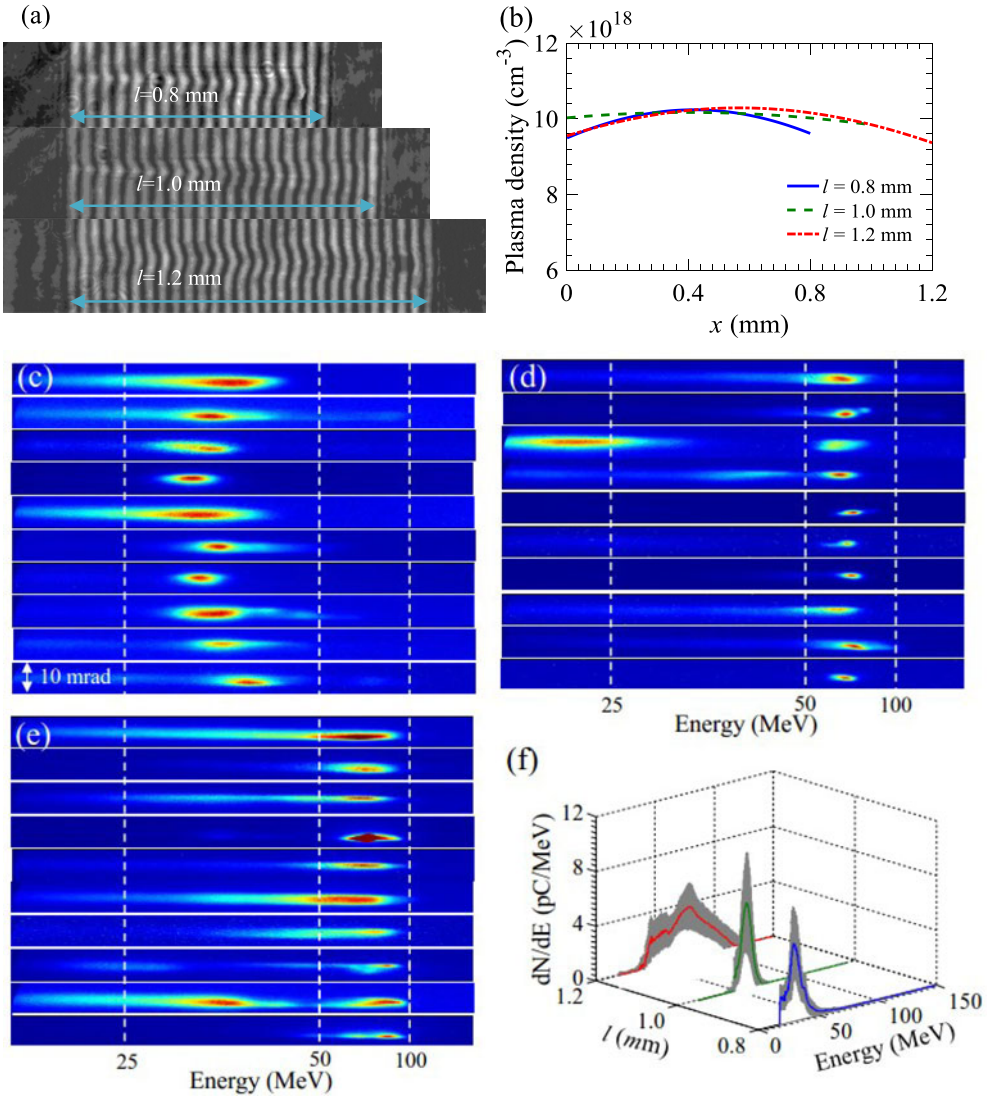

FIGURE 3. The snapshots of the measured interferogram (*a*) and the corresponding plasma density profile with different l (*b*). (*c–e*) Spectrometer images of ten shots for each of three different runs with different l of 0.8 mm (*c*), 1.0 mm (*d*) and 1.2 mm (*e*) from the LWFA. (*f*) Average integrated lineout and root-mean-square (grey area) of these shots.

low energy were first removed for the multi-bunch shots, and then the average was performed. Since the later injected e-bunches (Corde *et al.* 2013) which are located behind have no influence on the acceleration of the first injected bunches, for the multi-bunch shots, the obtained e-bunches with a much broader spectrum at the low energy level were not counted. The increase of the peak energy ε_p while lengthening the distance l indicated that the e-bunches witness a continuous acceleration before $l = 1.2$ mm. Meanwhile, the energy spread decreased from 5.7 to 3.4 MeV while the corresponding l changed from 0.8 to 1.0 mm, and then increased to 13.4 MeV while l was increases to 1.2 mm. This energy spread compression at first and then the

https://doi.org/10.1017/S0022377818001356 Published online by Cambridge University Press

l (mm)	ε_p (MeV)	r.m.s. $\lvert\Delta\varepsilon\rvert$ (MeV)	Q_1 (pC)	Q_2 (pC)
0.8	31.4 ± 2.1	5.7 ± 1.9	27.5 ± 10.8	27.5 ± 10.8
1.0	61.5 ± 2.5	3.4 ± 2.0	32.8 ± 11.5	52.9 ± 34.2
1.2	77.7 ± 3.1	13.4 ± 2.6	40.6 ± 18.2	90.9 ± 45.1

TABLE 1. Comparison of e-bunch spectral parameters with different l.

Case	E (V m^{-2})	ΔE_x (V m^{-1})	l_b (μm)
Experiment	$(4.1 \pm 1.9) \times 10^{16}$	$(4.8 \pm 0.9) \times 10^{10}$	1.2 ± 0.6
Simulation	7.0×10^{16}	6.3×10^{10}	0.9

TABLE 2. Comparison of wakefield and e-bunch parameters between experiment and simulation.

broadening during the acceleration were caused by the phase space rotation of the accelerated e-bunch in a wakefield. The energy chirp compensation obtained during the early acceleration, which is critical for acceleration optimization in a LWFA, could be applied for high-quality e-bunch generation such as compressing the relative energy spread of the accelerated e-bunch to the one thousandth level (Brinkmann *et al.* 2017; Manahan *et al.* 2017). Moreover, the obtained charge of the targeted e-bunch Q_1 and the whole spectrum Q_2 with different l were listed, a larger Q_2 compared with Q_1 at $l = 1.0$ mm and 1.2 mm suggested the existence of the later injected e-bunches at around $l = 1.0$ mm.

Since the energy spread $\Delta\varepsilon$ is defined as $\Delta\varepsilon = \varepsilon_{\text{front}} - \varepsilon_{\text{back}}$, $\Delta\varepsilon > 0$ ($\Delta\varepsilon < 0$) for e-bunches with negative (positive) energy chirp, the sign of $\Delta\varepsilon$ should be properly judged as the spectra only give the absolute values. Since the wakefield is supposed to be linear and the wakefield dispersion for the e-bunch ΔE_x stays constant during the acceleration, the variation of $\Delta\varepsilon$ should be proportional to the acceleration length. Hence,

$$\frac{\Delta\varepsilon_2 - \Delta\varepsilon_1}{l_{a1}} \approx \frac{\Delta\varepsilon_3 - \Delta\varepsilon_2}{l_{a2}}, \tag{3.1}$$

where $l_{a1} = l_2 - l_1$, $l_{a2} = l_3 - l_2$, $l_1 = 0.8$ mm, $l_2 = 1.0$ mm and $l_3 = 1.2$ mm. Moreover, the fact that the evolution of the energy spread undergoes a compression at first and then a growth indicates that the energy chirp of the e-bunch is negative ($\Delta\varepsilon > 0$) when $l = 0.8$ mm. Therefore, the energy spread $\Delta\varepsilon$ should be given as: $\Delta\varepsilon_1 = (5.7 \pm 2.2)$ MeV, $\Delta\varepsilon_2 = (-3.4 \pm 2.0)$ MeV, $\Delta\varepsilon_3 = (-13.4 \pm 2.9)$ MeV. Then the wakefield parameters such as E, ΔE_x and the e-bunch length l_b could be estimated by integrating equations (2.1)–(2.5) together with (3.1); the results are listed in table 2, l_b and the corresponding ΔE_x are r.m.s. values since the e-bunch energy spread applied in our estimations were r.m.s. values. Therefore, we can gain insight into the longitudinal bunch dynamics in the plasma wake and predict the e-bunch performance in further acceleration. Compared with other LWFA experiments which explore the energy spectrum evolution during the self-injection and acceleration processes (Hsieh *et al.* 2006; Kim *et al.* 2017), the e-bunch phase space rotation was obtained and an important wake (e-bunch) parameter E (l_b) was estimated in a simple way in our results. There are also some works dealing with the e-bunch phase

https://doi.org/10.1017/S0022377818001356 Published online by Cambridge University Press

space rotation in a wakefield with beam loading taken into account in the colliding pulse injection case (Rechatin *et al.* 2009*a*, 2010), and the nonlinear fields in their experiments resulted in much more complicated bunch dynamics.

4. Simulation results

In order to investigate the longitudinal dynamics of the e-bunch in the LWFA, and to further check out the accuracy of these estimations, we performed 3-D PIC simulations using the VORPAL code (Nieter & Cary 2004). The laser parameters listed in the caption of figure 4 were chosen to be close to the experimentally measured values, and the employed plasma density profile is presented in figure 4(*a*). The first injected e-bunch was self-injected with negative energy chirp into the plasma, and accelerated to a peak energy of 28.6 MeV with r.m.s. energy spread of 8.2 MeV at $x = 0.83$ mm, as shown in figure 4(*c*). Then, the e bunch was accelerated to 66.6 MeV at $x = 0.99$ mm and its energy chirp was compensated and start to reverse, meanwhile, its r.m.s. absolute energy spread was compressed to 2.8 MeV. After that, the bunch was accelerated to 89.5 MeV at $x = 1.19$ mm before dephasing, and its energy spread was over compensated while increasing to 12.4 MeV. The corresponding spectra shown in figure 4(*d*) revealed that the energy spread of the e-bunch was compensated and then enlarged due to the phase space rotation. It is noticeable that later injection occurred at $x = 0.99$ mm, and the energy of the later injected e bunches was always less than the first injected bunch before $x = 1.19$ mm. The total charge accelerated at the end of the simulation was 118.5 pC, and the charge of this first injected e-bunch was 46.2 pC, these results were consistent with the obtained charge in the experiment, as shown in table 1. Figure 4(*e*) shows the corresponding on-axis wakefield E_x at different propagation distances and the longitudinal profile of the accelerated e-bunch; it is clear that the located wakefields were approximately linear, and beam loading of the bunch was weak. This led to the phase space rotation of the bunch, then the energy spread compensation at the beginning of acceleration. The wakefield parameters (E' and ΔE_x are average values with a time span of 0.33 picosecond) and r.m.s. l_b values are listed in table 2, which are in good agreement with the experimental results.

Comparison of the spectral evolution between the PIC simulations and the experimental results are shown in figure 4(*f*), and the peak energy ε_p shows a discrepancy between the simulation and experiment as well as in the absolute energy spread $|\Delta\varepsilon|$. This could be attributed to the downward density ramp at the tail of the plasma, as mentioned above in the experiment. As shown in figure 4(*f*), the energy gain of the e-bunch in the simulation slowed down on propagating forward, thus the acceleration field was decreasing with the e-bunch dephasing. Therefore, the experimentally generated e-bunches with $l_1 = 0.8$ mm would be further accelerated in the plasma downward ramp even when the wakefield period expands rapidly. However, for the e-bunches with $l_3 = 1.2$ mm, these were decelerated in the plasma downward ramp and as such they were located at the deceleration phase. On the other hand, the absolute energy spread $|\Delta\varepsilon|$ caused by the wakefield dispersion varies less in the plasma downward ramp because ΔE_x decreased rapidly while the wake period expanded. Apart from the plasma density ramp in the experiment, there are some other factors which could also introduce uncertainties in the parameter estimations, such as deformation of the bubble during the acceleration (Kalmykov *et al.* 2011).

https://doi.org/10.1017/S0022377818001356 Published online by Cambridge University Press

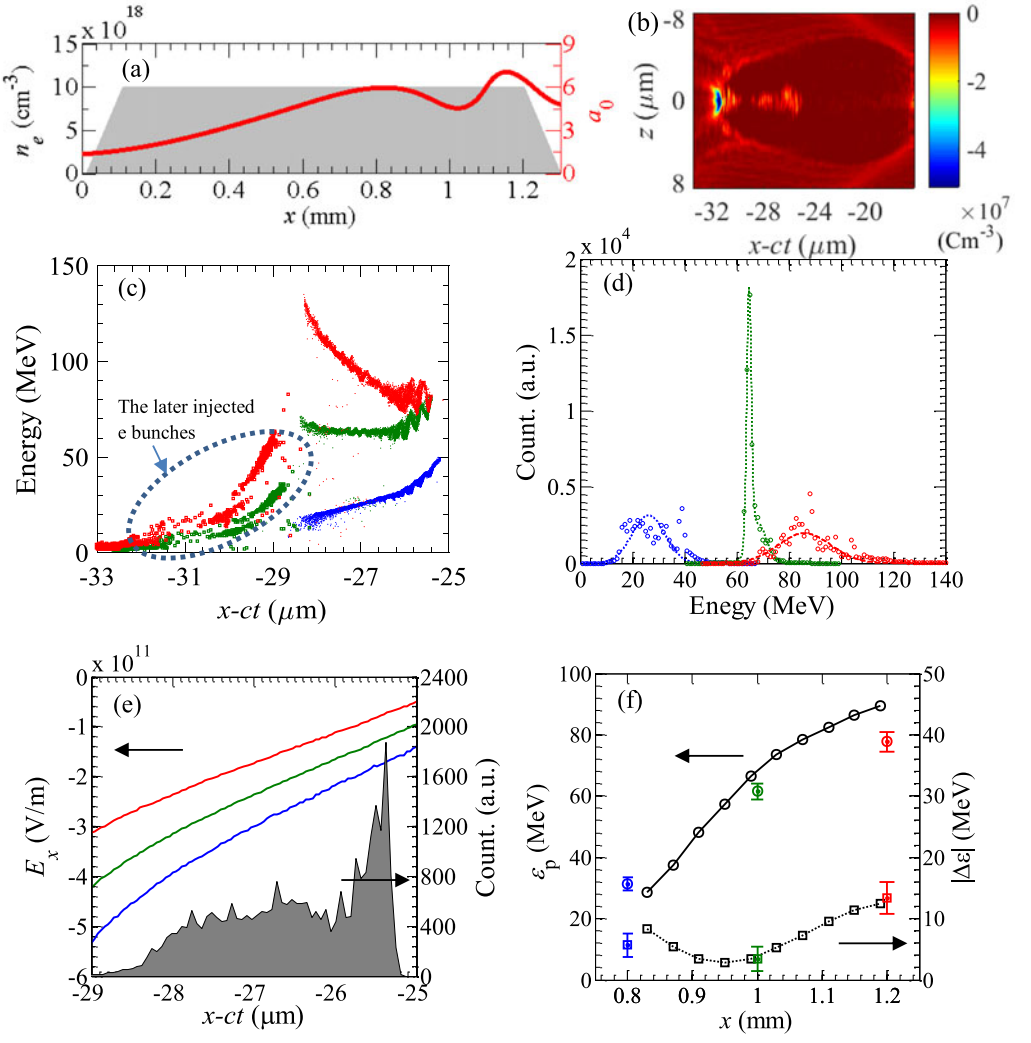

FIGURE 4. (*a*) Plasma density profile and laser amplitude a_0 evolution along the laser propagation direction x in the simulation. (*b*) Energy evolution (*c*) of the injected e-bunches along x and the corresponding energy spectra (*d*) of the first injected ones at different propagation distances, the dotted lines are the Gaussian fittings. (*e*) The on-axis wakefield E_x at different propagation distances together with the longitudinal profile of the accelerated e-bunch. The colours in (*c–e*) represent different propagation distances: $x = 0.83$ mm (blue), $x = 0.99$ mm (green) and $x = 1.19$ mm (red). (*f*) Comparison of the evolution of peak energy ε_p (○) and absolute energy spread $|\Delta\varepsilon|$ (□) between 3-D PIC simulations and the experimental results (with error bars). Laser parameters: wavelengths $\lambda_0 = 0.8$ μm, normalized amplitude $a_0 = 1.2$, pulse durations $\tau = 33$ fs and FWHM spot size $w_{\mathrm{FWHM}} = 32$ μm. The linearly polarized Gaussian pulse was focused at the starting position of the plasma. Simulation parameters: numerical grid's cell size $\Delta x \times \Delta y \times \Delta z = 0.04 \times 0.2 \times 0.2$ μm^3, moving window size $W_x \times W_y \times W_z = 42 \times 136 \times 136$ μm^3.

https://doi.org/10.1017/S0022377818001356 Published online by Cambridge University Press

5. Conclusion

In conclusion, we demonstrate the experimental observation of energy chirp compensation in a LWFA, and estimate the characteristic wake parameters which are correlated with the phase space rotation based on the evolution of energy spectra. These results reveal more details of the longitudinal dynamics of the accelerated e-bunch in a LWFA with the help of 3-D PIC simulation results, which will provide better control over a LWFA with tuneable ultrashort electron sources.

Acknowledgements

This work was supported by the National Natural Science Foundation of China (grant nos 11127901, 11425418, 61521093 and 11505263), Shanghai Sailing Program (grant no. 17YF1421100), Strategic Priority Research Program (B) (grant no. XDB16), Youth Innovation Promotion Association CAS and State Key Laboratory Program of the Chinese Ministry of Science and Technology.

REFERENCES

BONNET, T., COMET, M., DENIS-PETIT, D., GOBET, F., HANNACHI, F., TARISIEN, M., VERSTEEGEN, M. & ALEONARD, M. M. 2013 Response functions of imaging plates to photons, electrons and 4He particles. *Rev. Sci. Instrum.* **84**, 103510.

BOURGEOIS, N., COWLEY, J. & HOOKER, S. M. 2013 Two-pulse ionization injection into quasilinear laser wakefields. *Phys. Rev. Lett.* **111**, 155004.

BRINKMANN, R., DELBOS, N., DORNMAIR, I., KIRCHEN, M., ASSMANN, R., BEHRENS, C., FLOETTMANN, K., GREBENYUK, J., GROSS, M., JALAS, S. *et al.* 2017 Chirp mitigation of plasma-accelerated beams by a modulated plasma density. *Phys. Rev. Lett.* **118**, 214801.

BUCK, A., WENZ, J., XU, J., KHRENNIKOV, K., SCHMID, K., HEIGOLDT, M., MIKHAILOVA, J. M., GEISSLER, M., SHEN, B., KRAUSZ, F. *et al.* 2013 Shock-front injector for high-quality laser-plasma acceleration. *Phys. Rev. Lett.* **110**, 185006.

CHEN, S., POWERS, N. D., GHEBREGZIABHER, I., MAHARJAN, C. M., LIU, C., GOLOVIN, G., BANERJEE, S., ZHANG, J., CUNNINGHAM, N., MOORTI, A. *et al.* 2013 MeV-energy X rays from inverse compton scattering with laser-wakefield accelerated electrons. *Phys. Rev. Lett.* **110**, 155003.

CORDE, S., THAURY, C., LIFSCHITZ, A., LAMBERT, G., TA PHUOC, K., DAVOINE, X., LEHE, R., DOUILLET, D., ROUSSE, A. & MALKA, V. 2013 Observation of longitudinal and transverse self-injections in laser-plasma accelerators. *Nat. Commun.* **4**, 1501.

FAURE, J., RECHATIN, C., LUNDH, O., AMMOURA, L. & MALKA, V. 2010 Injection and acceleration of quasimonoenergetic relativistic electron beams using density gradients at the edges of a plasma channel. *Phys. Plasmas* **17**, 083107.

FAURE, J., RECHATIN, C., NORLIN, A., LIFSCHITZ, A., GLINEC, Y. & MALKA, V. 2006 Controlled injection and acceleration of electrons in plasma wakefields by colliding laser pulses. *Nature* **444**, 737.

FUCHS, M., WEINGARTNER, R., POPP, A., MAJOR, Z., BECKER, S., OSTERHOFF, J., CORTRIE, I., ZEITLER, B., HORLEIN, R., TSAKIRIS, G. D. *et al.* 2009 Laser-driven soft-X-ray undulator source. *Nat. Phys.* **5**, 826.

GEDDES, C. G. R., NAKAMURA, K., PLATEAU, G. R., TOTH, C., CORMIER-MICHEL, E., ESAREY, E., SCHROEDER, C. B., CARY, J. R. & LEEMANS, W. P. 2008 Plasma-density-gradient injection of low absolute-momentum-spread electron bunches. *Phys. Rev. Lett.* **100**, 215004.

GONSALVES, A. J., NAKAMURA, K., LIN, C., PANASENKO, D., SHIRAISHI, S., SOKOLLIK, T., BENEDETTI, C., SCHROEDER, C. B., GEDDES, C. G. R., VAN TILBORG, J. *et al.* 2011 Tunable laser plasma accelerator based on longitudinal density tailoring. *Nat. Phys.* **7**, 862.

HEIGOLDT, M., POPP, A., KHRENNIKOV, K., WENZ, J., CHOU, S. W., KARSCH, S., BAJLEKOV, S. I., HOOKER, S. M. & SCHMIDT, B. 2015 Temporal evolution of longitudinal bunch profile in a laser wakefield accelerator. *Phys. Rev. Spec. Top.* **18**, 121302.

HSIEH, C. T., HUANG, C. M., CHANG, C. L., HO, Y. C., CHEN, Y. S., LIN, J. Y., WANG, J. & CHEN, S. Y. 2006 Tomography of injection and acceleration of monoenergetic electrons in a laser-wakefield accelerator. *Phys. Rev. Lett.* **96**, 095001.

HUANG, Z., DING, Y. & SCHROEDER, C. B. 2012 Compact X-ray free-electron laser from a laser-plasma accelerator using a transverse-gradient undulator. *Phys. Rev. Lett.* **109**, 204801.

JAROSZYNSKI, D. A., BINGHAM, R., BRUNETTI, E., ERSFELD, B., GALLACHER, J., VAN DER GEER, B., ISSAC, R., JAMISON, S. P., JONES, D., DE LOOS, M. *et al.* 2006 Radiation sources based on laser-plasma interactions. *Phil. Trans. R. Soc. Lond.* A **364**, 689.

KALMYKOV, S. Y., BECK, A., YI, S. A., KHUDIK, V. N., DOWNER, M. C., LEFEBVRE, E., SHADWICK, B. A. & UMSTADTER, D. P. 2011 Electron self-injection into an evolving plasma bubble: quasi-monoenergetic laser-plasma acceleration in the blowout regime. *Phys. Plasmas* **18**, 056704.

KALMYKOV, S. Y., DAVOINE, X., LEHE, R., LIFSCHITZ, A. F. & SHADWICK, B. A. 2015 Optical control of electron phase space in plasma accelerators with incoherently stacked laser pulses. *Phys. Plasmas* **22**, 056701.

KIM, H. T., PAE, K. H., CHA, H. J., KIM, I. J., YU, T. J., SUNG, J. H., LEE, S. K., JEONG, T. M. & LEE, J. 2013 Enhancement of electron energy to the multi-GeV regime by a dual-stage laser-wakefield accelerator pumped by petawatt laser pulses. *Phys. Rev. Lett.* **111**, 165002.

KIM, H. T., PATHAK, V. B., HONG PAE, K., LIFSCHITZ, A., SYLLA, F., SHIN, J. H., HOJBOTA, C., LEE, S. K., SUNG, J. H., LEE, H. W. *et al.* 2017 Stable multi-GeV electron accelerator driven by waveform-controlled PW laser pulses. *Sci. Rep.* **7**, 10203.

KOSTYUKOV, I., PUKHOV, A. & KISELEV, S. 2004 Phenomenological theory of laser-plasma interaction in 'bubble' regime. *Phys. Plasmas* **11**, 5256.

LEEMANS, W. P., GONSALVES, A. J., MAO, H. S., NAKAMURA, K., BENEDETTI, C., SCHROEDER, C. B., TH, T., DANIELS, C., MITTELBERGER, J., BULANOV, D. E. *et al.* 2014 Multi-GeV electron beams from capillary-discharge-guided subpetawatt laser pulses in the self-trapping regime. *Phys. Rev. Lett.* **113**, 245002.

LITOS, M., ADLI, E., AN, W., CLARKE, C. I., CLAYTON, C. E., CORDE, S., DELAHAYE, J. P., ENGLAND, R. J., FISHER, A. S., FREDERICO, J. *et al.* 2014 High-efficiency acceleration of an electron beam in a plasma wakefield accelerator. *Nature* **515**, 92.

LIU, J. S., XIA, C. Q., WANG, W. T., LU, H. Y., WANG, C., DENG, A. H., LI, W. T., ZHANG, H., LIANG, X. Y., LENG, Y. X. *et al.* 2011 All-optical cascaded laser wakefield accelerator using ionization-induced injection. *Phys. Rev. Lett.* **107**, 035001.

LU, H., LIU, M., WANG, W., WANG, C., LIU, J., DENG, A., XU, J., XIA, C., LI, W., ZHANG, H. *et al.* 2011 Laser wakefield acceleration of electron beams beyond 1 GeV from an ablative capillary discharge waveguide. *Appl. Phys. Lett.* **99**, 091502.

LU, W., TZOUFRAS, M., JOSHI, C., TSUNG, F. S., MORI, W. B., VIEIRA, J., FONSECA, R. A. & SILVA, L. O. 2007 Generating multi-GeV electron bunches using single stage laser wakefield acceleration in a 3D nonlinear regime. *Phys. Rev. Spec. Top.* **10**, 061301.

MANAHAN, G. G., HABIB, A. F., SCHERKL, P., DELINIKOLAS, P., BEATON, A., KNETSCH, A., KARGER, O., WITTIG, G., HEINEMANN, T., SHENG, Z. M. *et al.* 2017 Single-stage plasma-based correlated energy spread compensation for ultrahigh 6D brightness electron beams. *Nat. Commun.* **8**, 15705.

NIETER, C. & CARY, J. R. 2004 VORPAL: a versatile plasma simulation code. *J. Comput. Phys.* **196**, 448.

OZ, E., DENG, S., KATSOULEAS, T., MUGGLI, P., BARNES, C., BLUMENFELD, I., DECKER, F., EMMA, P., HOGAN, M., ISCHEBECK, R. *et al.* 2007 Ionization-induced electron trapping in ultrarelativistic plasma wakes. *Phys. Rev. Lett.* **98**, 084801.

PAK, A., MARSH, K. A., MARTINS, S. F., LU, W., MORI, W. B. & JOSHI, C. 2010 Injection and trapping of tunnel-ionized electrons into laser-produced wakes. *Phys. Rev. Lett.* **104**, 025003.

PHUOC, K. T., CORDE, S., THAURY, C., MALKA, V., TAFZI, A., GODDET, J. P., SHAH, R. C., SEBBAN, S. & ROUSSE, A. 2012 All-optical compton gamma-ray source. *Nat. Photon.* **6**, 308.

POLLOCK, B. B., CLAYTON, C. E., RALPH, J. E., ALBERT, F., DAVIDSON, A., DIVOL, L., FILIP, C., GLENZER, S. H., HERPOLDT, K., LU, W. *et al.* 2011 Demonstration of a narrow energy spread, approximately 0.5 GeV electron beam from a two-stage laser wakefield accelerator. *Phys. Rev. Lett.* **107**, 045001.

POWERS, N. D., GHEBREGZIABHER, I., GOLOVIN, G., LIU, C., CHEN, S., BANERJEE, S., ZHANG, J. & UMSTADTER, D. P. 2014 Quasi-monoenergetic and tunable X-rays from a laser-driven Compton light source. *Nat. Photon.* **8**, 29.

RECHATIN, C., DAVOINE, X., LIFSCHITZ, A., ISMAIL, A. B., LIM, J., LEFEBVRE, E., FAURE, J. & MALKA, V. 2009*a* Observation of beam loading in a laser-plasma accelerator. *Phys. Rev. Lett.* **103**, 194804.

RECHATIN, C., FAURE, J., BEN-ISMAIL, A., LIM, J., FITOUR, R., SPECKA, A., VIDEAU, H., TAFZI, A., BURGY, F. & MALKA, V. 2009*b* Controlling the phase-space volume of injected electrons in a laser-plasma accelerator. *Phys. Rev. Lett.* **102**, 164801.

RECHATIN, C., FAURE, J., DAVOINE, X., LUNDH, O., LIM, J., BEN-ISMAÏL, A., BURGY, F., TAFZI, A., LIFSCHITZ, A., LEFEBVRE, E. *et al.* 2010 Characterization of the beam loading effects in a laser plasma accelerator. *New J. Phys.* **12**, 045023.

SCHLENVOIGT, H. P., HAUPT, K., DEBUS, A., BUDDE, F., CKEL, J., PFOTENHAUER, O., SCHWOERER, S., ROHWER, H., GALLACHER, E., BRUNETTI, J. G. *et al.* 2007 A compact synchrotron radiation source driven by a laser-plasma wakefield accelerator. *Nat. Phys.* **4**, 130.

SCHWOERER, H., LIESFELD, B., SCHLENVOIGT, H. P., AMTHOR, K. U. & SAUERBREY, R. 2006 Thomson-backscattered X rays from laser-accelerated electrons. *Phys. Rev. Lett.* **96**, 014802.

STEINKE, S., VAN TILBORG, J., BENEDETTI, C., GEDDES, C. G., SCHROEDER, C. B., DANIELS, J., SWANSON, K. K., GONSALVES, A. J., NAKAMURA, K., MATLIS, N. H. *et al.* 2016 Multistage coupling of independent laser-plasma accelerators. *Nature* **530**, 190.

TAJIMA, T. & DAWSON, J. M. 1979 Laser electron accelerator. *Phys. Rev. Lett.* **43**, 267.

TSUNG, F. S., NARANG, R., MORI, W. B., JOSHI, C., FONSECA, R. A. & SILVA, L. O. 2004 Near-GeV-energy laser-wakefield acceleration of self-injected electrons in a centimeter-scale plasma channel. *Phys. Rev. Lett.* **93**, 185002.

TZOUFRAS, M., LU, W., TSUNG, F. S., HUANG, C., MORI, W. B., KATSOULEAS, T., VIEIRA, J., FONSECA, R. A. & SILVA, L. O. 2008 Beam loading in the nonlinear regime of plasma-based acceleration. *Phys. Rev. Lett.* **101**, 145002.

WANG, W., LI, W., LIU, J., WANG, C., CHEN, Q., ZHANG, Z., QI, R., LENG, Y., LIANG, X., LIU, Y. *et al.* 2013*a* Control of seeding phase for a cascaded laser wakefield accelerator with gradient injection. *Appl. Phys. Lett.* **103**, 243501.

WANG, X., ZGADZAJ, R., FAZEL, N., LI, Z., YI, S. A., ZHANG, X., HENDERSON, W., CHANG, Y. Y., KORZEKWA, R., TSAI, H. E. *et al.* 2013*b* Quasi-monoenergetic laser-plasma acceleration of electrons to 2 GeV. *Nat. Commun.* **4**, 1988.

XI, Y., HIDDING, B., BRUHWILER, D., PRETZLER, G. & ROSENZWEIG, J. B. 2013 Hybrid modeling of relativistic underdense plasma photocathode injectors. *Phys. Rev. Spec. Top.* **16**, 031303.

XU, Y., LU, J., LI, W., WU, F., LI, Y., WANG, C., LI, Z., LU, X., LIU, Y., LENG, Y. *et al.* 2016 A Stable 200 TW/1 Hz Ti:sapphire laser for driving full coherent XFEL. *Opt. Laser Technol.* **79**, 141.

ZENG, M., CHEN, M., YU, L. L., MORI, W. B., SHENG, Z. M., HIDDING, B., JAROSZYNSKI, D. A. & ZHANG, J. 2015 Multichromatic Narrow-Energy-Spread Electron Bunches from Laser-Wakefield Acceleration with Dual-Color Lasers. *Phys. Rev. Lett.* **114**, 084801.

ZHANG, Z., LIU, J., WANG, W., LI, W., YU, C., TIAN, Y., QI, R., WANG, C., QIN, Z., FANG, M. *et al.* 2015 Generation of high quality electron beams from a quasi-phase-stable cascaded laser wakefield accelerator with density-tailored plasma segments. *New J. Phys.* **17**, 103011.

ZHANG, Z. J., LI, W. T., LIU, J. S., WANG, W. T., YU, C. H., TIAN, Y., NAKAJIMA, K., DENG, A. H., QI, R., WANG, C. *et al.* 2016 Energy spread minimization in a cascaded laser wakefield accelerator via velocity bunching. *Phys. Plasmas* **23**, 053106.

ZHOU, Z., LIU, J., LU, H., WANG, Z., JU, J., WANG, C., XIA, C., WANG, W., DENG, A., XU, Y. *et al.* 2010 Propagation effects on fusion neutron generation in the Coulomb explosion of deuterated methane clusters. *J. Phys.* B **43**, 135603.

https://doi.org/10.1017/S0022377818001356 Published online by Cambridge University Press